Electronic Supplementary Material (ESI) for Soft Matter.

Electronic Supplementary Information for:

Hysteretic Memory in pH-Response of Water Contact Angle on Poly(acrylic acid) Brushes

Vivek Yadav, Adrienne V. Harkin, Megan L. Robertson,* and Jacinta C. Conrad*

Department of Chemical and Biomolecular Engineering

University of Houston, Houston, TX 77204-4004

*E-mail: mlrobertson@uh.edu, jcconrad@uh.edu

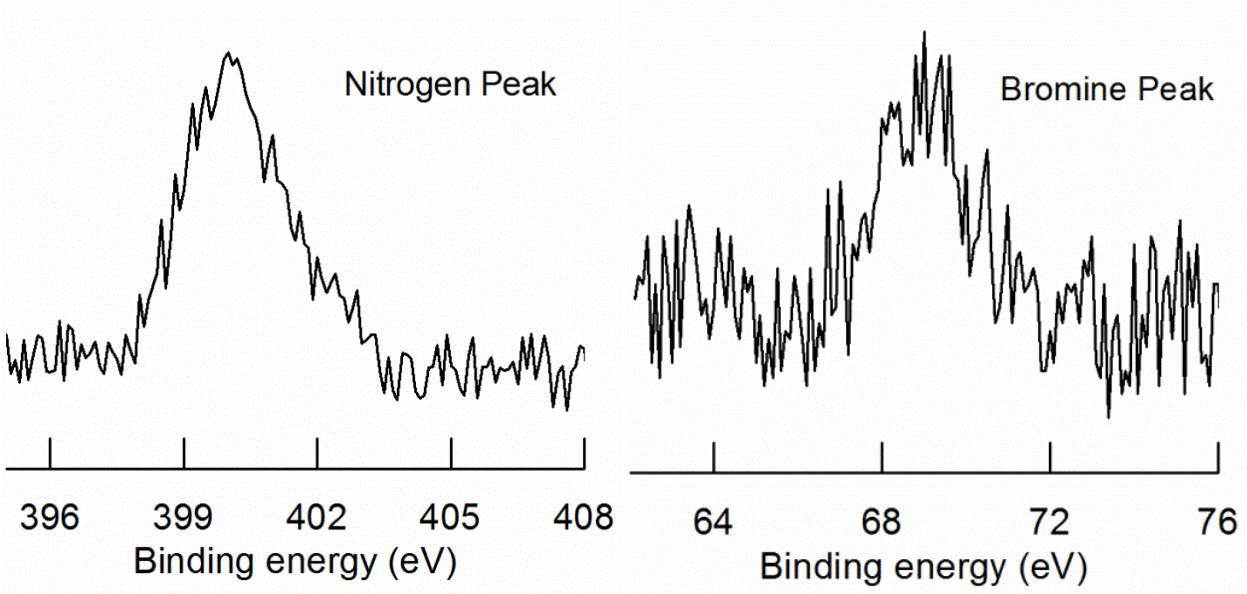

Figure S1. XPS spectra obtained after APTES deposition and initiator attachment on silicon substrate. The presence of nitrogen and bromine peak confirms successful grafting of APTES and surface initiator to the silicon substrate, consistent with ref. [1].

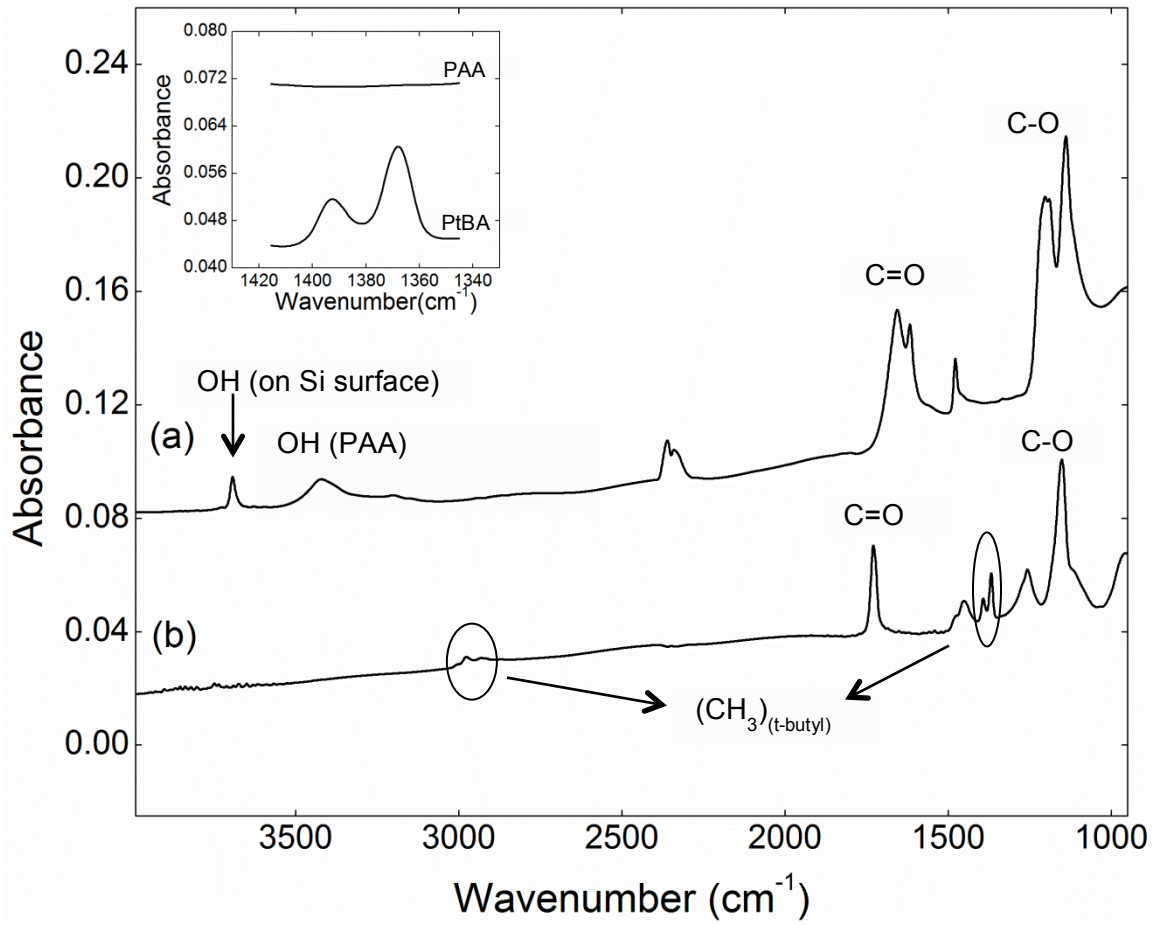

Figure S2. FTIR spectra of (a) PAA brush (thickness = 58 nm) and (b) PtBA brush (thickness = 65 nm). The conversion of PtBA to PAA is confirmed by i) disappearance of peaks located at 2977 and 1392/1368 cm^{-1} (associated with asymmetric stretching and bending, respectively, of the methyl group located on the t-butyl group) and ii) appearance of broad peak at 3420 cm^{-1} (associated with stretching of the OH group on PAA). The y-axis of the PAA spectrum is offset by 0.08 to allow the two spectra to be readily distinguished. The inset shows the complete disappearance of the PtBA peaks at 1392/1368 cm^{-1}, indicating that the conversion of PtBA brush to PAA brush is 100%. The y-axis of the PAA spectrum in the inset is offset by 0.03. FTIR peak assignments are consistent with refs. [2-10]

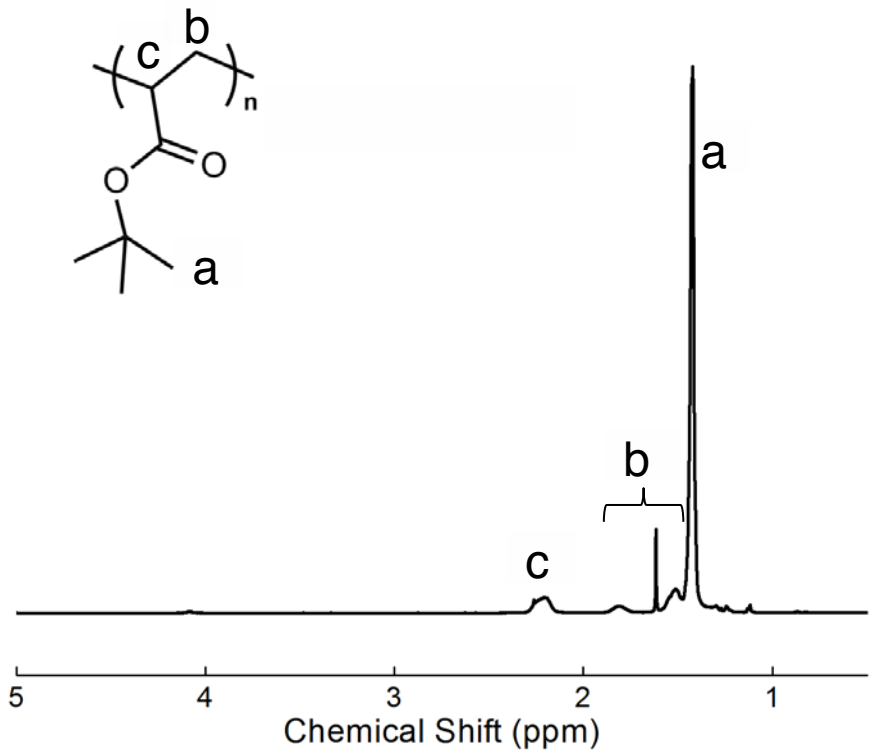

Figure S3. ^{1}H-NMR spectrum for PtBA polymerized in solution (M_n = 9,584, $Đ$ = 1.10). The ratio of (peak a + peak b) / (peak c) was 10.6 (theoretical value = 11). ^{1}H-NMR peak assignments ($CDCl_3$, δ, ppm): 2.08 – 2.32 (br, methine C**H** of the polymer backbone), 1.72 – 1.90 (br, meso methylene C$\mathbf{H}_2$ of the polymer backbone), 1.28 – 1.69 (br, meso, and racemo C$\mathbf{H}_2$ of the polymer backbone), 1.20-1.67 (br, $(C\mathbf{H}_3)_3C$). In the range of 1.20 – 1.70 ppm, peaks were deconvoluted using the mixed Gaussian and Lorentzian function in the Jeol software. Peak identifications are from refs. [11-14].

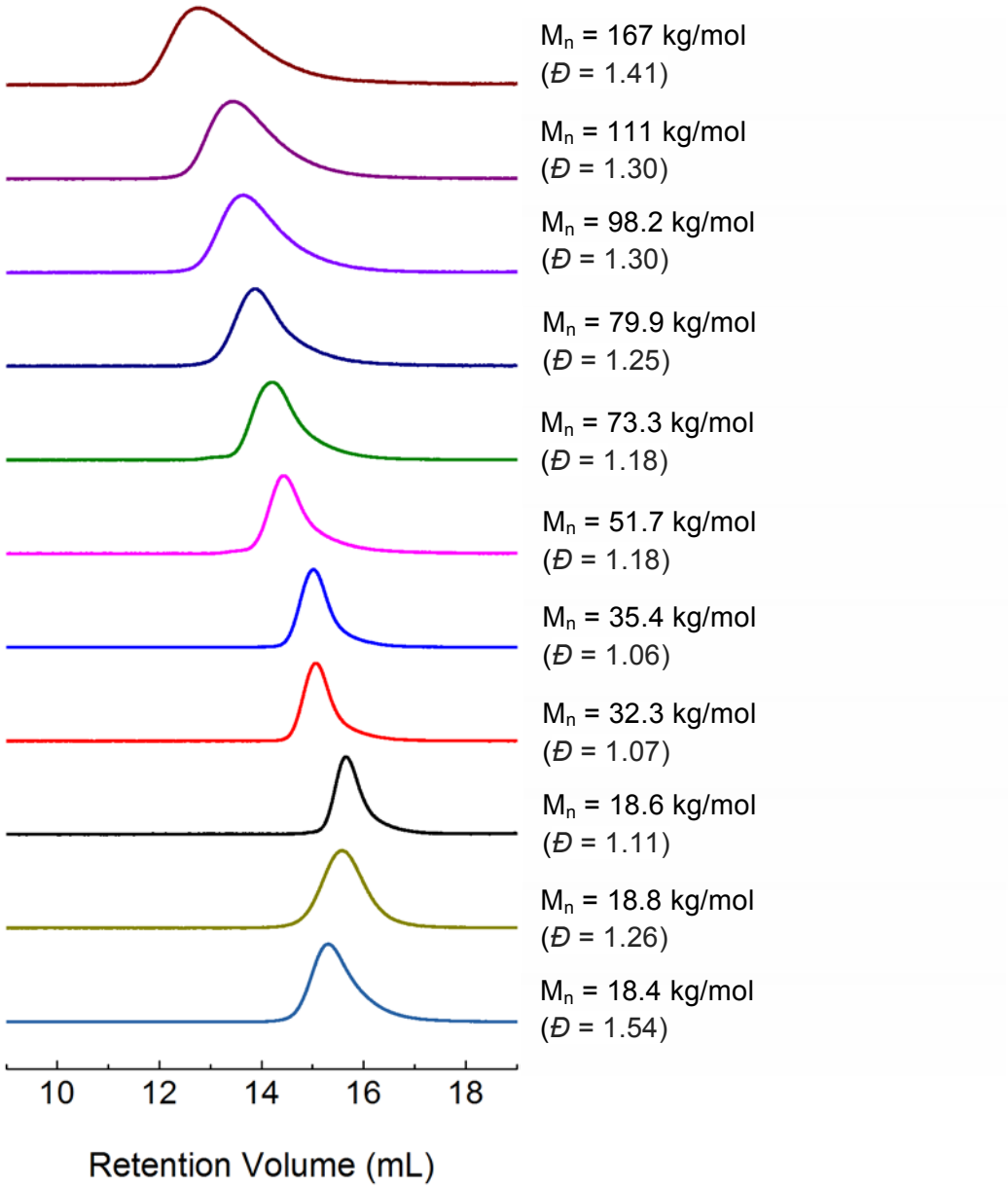

Figure S4. GPC refractometer data for PtBA polymerized in solution, concurrent with the synthesis of PtBA brushes on silicon substrates. Molecular weight and dispersity for each polymer are given in Table S1. The PtBA polymer with M_n = 18.8 kg/mol and *Đ* = 1.26 was synthesized with a higher ratio of initiator to catalyst and ligand (to increase the dispersity). The PtBA polymer with M_n = 18.4 kg/mol and *Đ* = 1.54 was synthesized with the addition of phenylhydrazine (also to increase the dispersity).

Table S1. Average as-synthesized dry thickness (with standard deviation) of each PtBA and PAA brush reported in the main text, corresponding molecular weight and dispersity of the PtBA that was polymerized in solution simultaneously during the PtBA brush synthesis, and reduction in brush thickness upon hydrolysis to PAA. The PtBA polymer with M_n = 18.8 kg/mol and $Đ$ = 1.26 was synthesized with a higher ratio of initiator to catalyst and ligand (to increase the dispersity). The PtBA polymer with M_n = 18.4 kg/mol and $Đ$ = 1.54 was synthesized with the addition of phenylhydrazine (also to increase the dispersity).

Average PtBA Brush Thickness (nm)	**M_n (kg/mol) of Solution PtBA ($Đ$)**	**Average PAA Brush Thickness (nm)**	**Reduction in PtBA Brush Thickness Upon Hydrolysis to PAA**
13.4 ± 0.3	18.6 (1.11)	6.8 ± 0.2	49.2 %
12.7 ± 0.3	18.8 (1.26)	6.3 ± 0.2	50.0 %
14.4 ± 0.3	18.4 (1.54)	7.3 ± 0.1	49.3 %
21.2 ± 0.3	32.3 (1.07)	10.6 ± 0.1	50.0 %
22.4 ± 0.1	35.4 (1.06)	11.7 ± 0.3	47.7 %
32.3 ± 0.4	51.7 (1.18)	15.2 ± 0.3	52.9 %
42.3 ± 0.6	73.3 (1.18)	20.1 ± 0.1	52.4 %
47.8 ± 0.7	79.9 (1.25)	22.2 ± 0.8	53.6 %
57.7 ± 0.6	98.2 (1.30)	27.2 ± 0.6	52.8 %
65.7 ± 0.6	111 (1.30)	30.4 ± 0.4	53.7 %
100.1 ± 0.7	167 (1.41)	44.2 ± 0.3	55.8 %

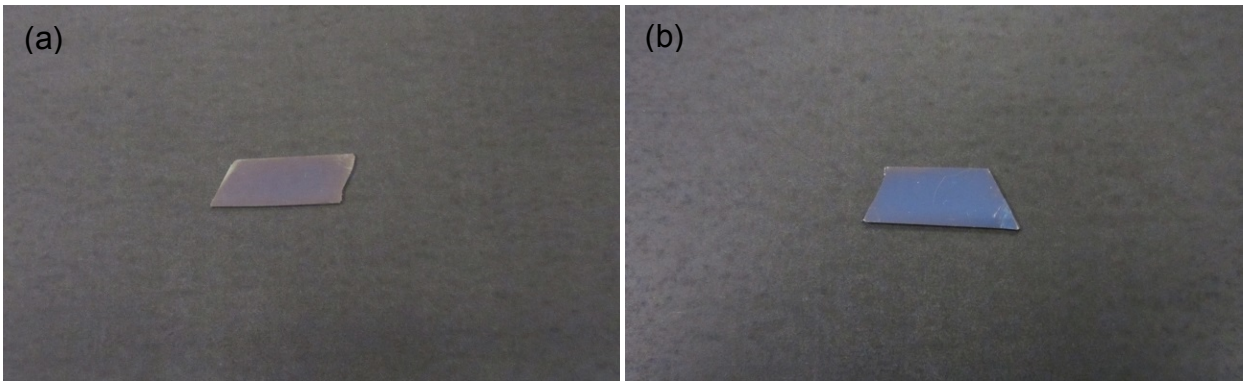

Figure S5. Camera images showing PtBA brushes of thickness (a) 85 nm and (b) 99 nm grafted on Si wafer. Different colors correspond to different brush thicknesses. Uniform brush color shows uniform brush thickness.

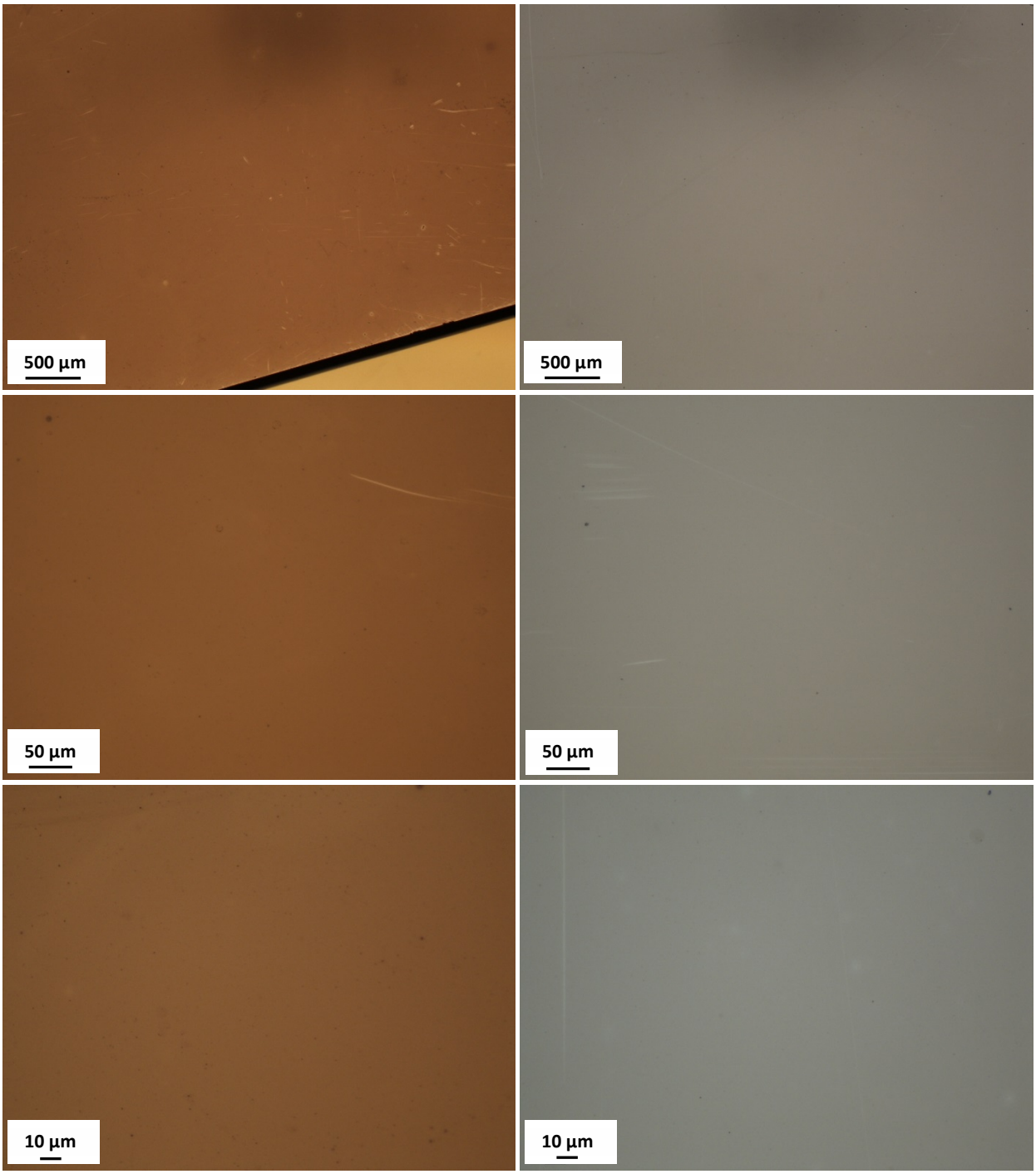

Figure S6. Optical microscopy images of a 69-nm thick PtBA brush (left column) and a 30-nm thick PAA brush (right column) at different magnifications. All brushes are uniform on the microscale. The scratches seen in the images arise from collisions of the stir bar with the surface during the reaction.

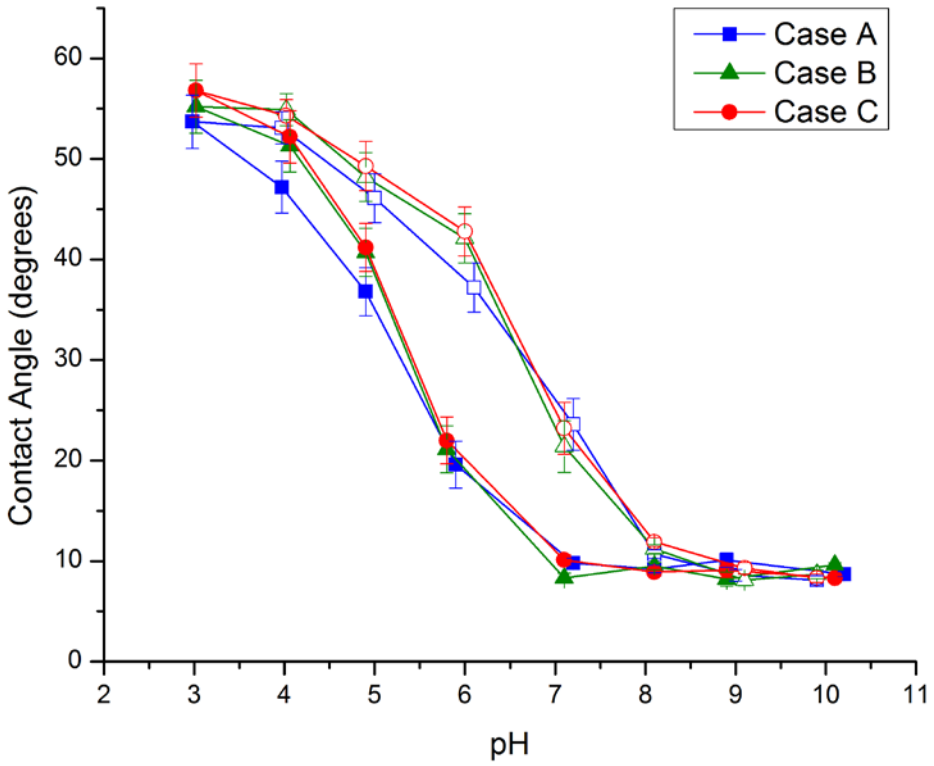

Figure S7. Contact angle as a function of pH for a PAA brush (as-synthesized dry thickness = 27 nm, grafting density = 0.39 chains/nm^2). Measurements were conducted under the following conditions: Case A) brush was soaked in a phosphate-buffered solution (ionic strength 0.05 M), and a drop of the same buffered solution was used for the contact angle measurement; Case B) brush was soaked in a non-buffered solution, and a DI water drop was used for the contact angle measurement; and Case C) brush was soaked in a non-buffered solution, and drop of the same non-buffered solution was used for the contact angle measurement. All three measurements agree within experimental errors at each pH, confirming that the contact angle measurement is robust.

Table S2. pK_a values for the measurement conditions investigated in Figure S5. The pK_a was measured for each case described in Figure S5 by fitting a sigmoidal function to the contact angle as a function of pH for both increasing and decreasing pH. The pK_a values obtained from the fits are indistinguishable within the measurement error.

Measurement Protocol	Soaking Solution	Drop Used for Contact Angle Measurement	pK_a Upon Decreasing pH	pK_a Upon Increasing pH
Case A	Buffered	Buffered	4.9 ± 0.2	6.1 ± 0.2
Case B	Non-buffered	DI water	5.0 ± 0.2	6.2 ± 0.2
Case C	Non-buffered	Non-buffered	4.9 ± 0.1	6.2 ± 0.1

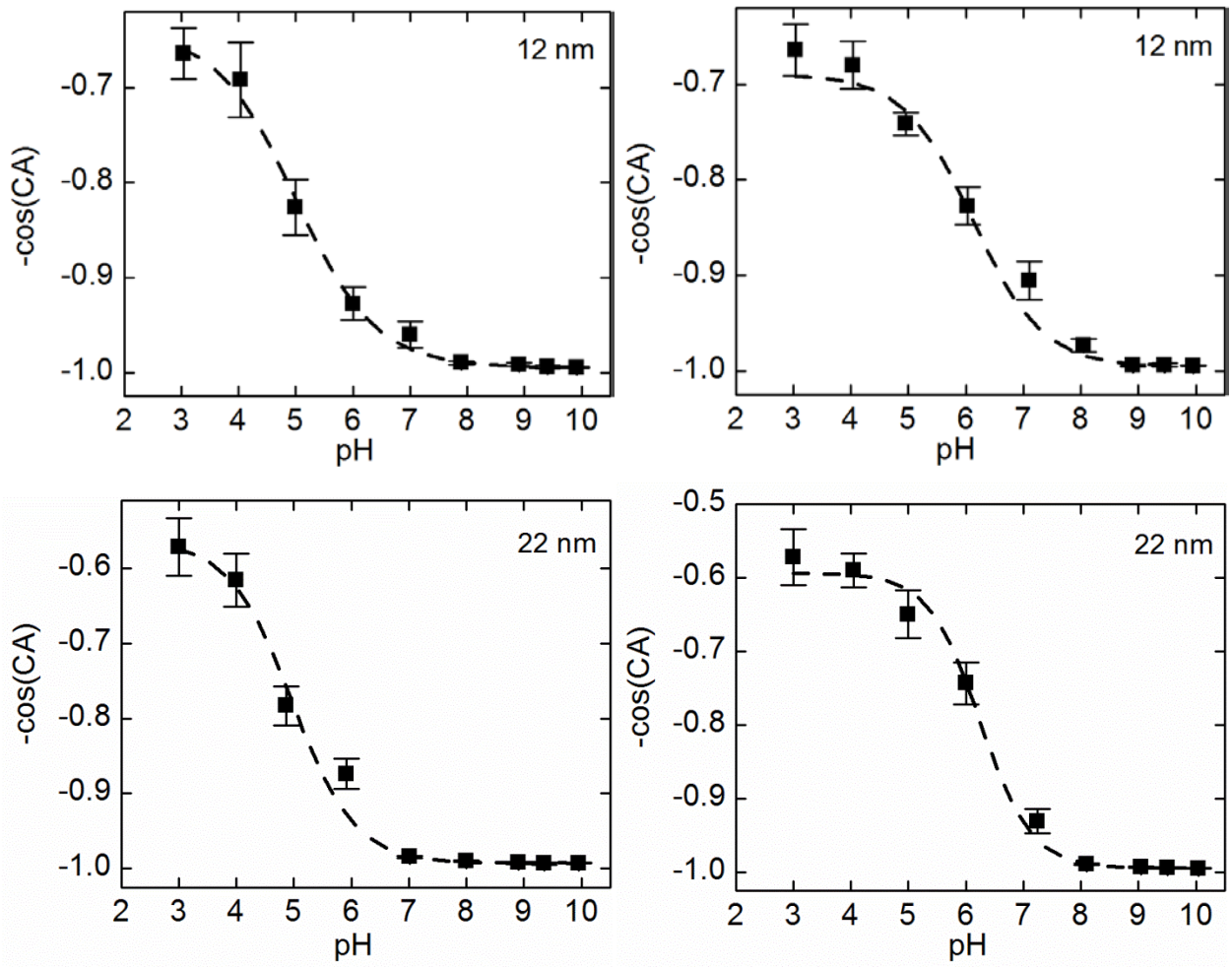

Figure S8. –cos(CA) as a function of pH for each brush thickness reported in Figure 2 (CA is the static water contact angle). Dry thickness (as-synthesized) is specified on each plot. In each pair of plots for a single thickness, the left graph corresponds to decreasing pH and the right graph corresponds to increasing pH. The dashed curves indicate sigmoidal fits to the data.

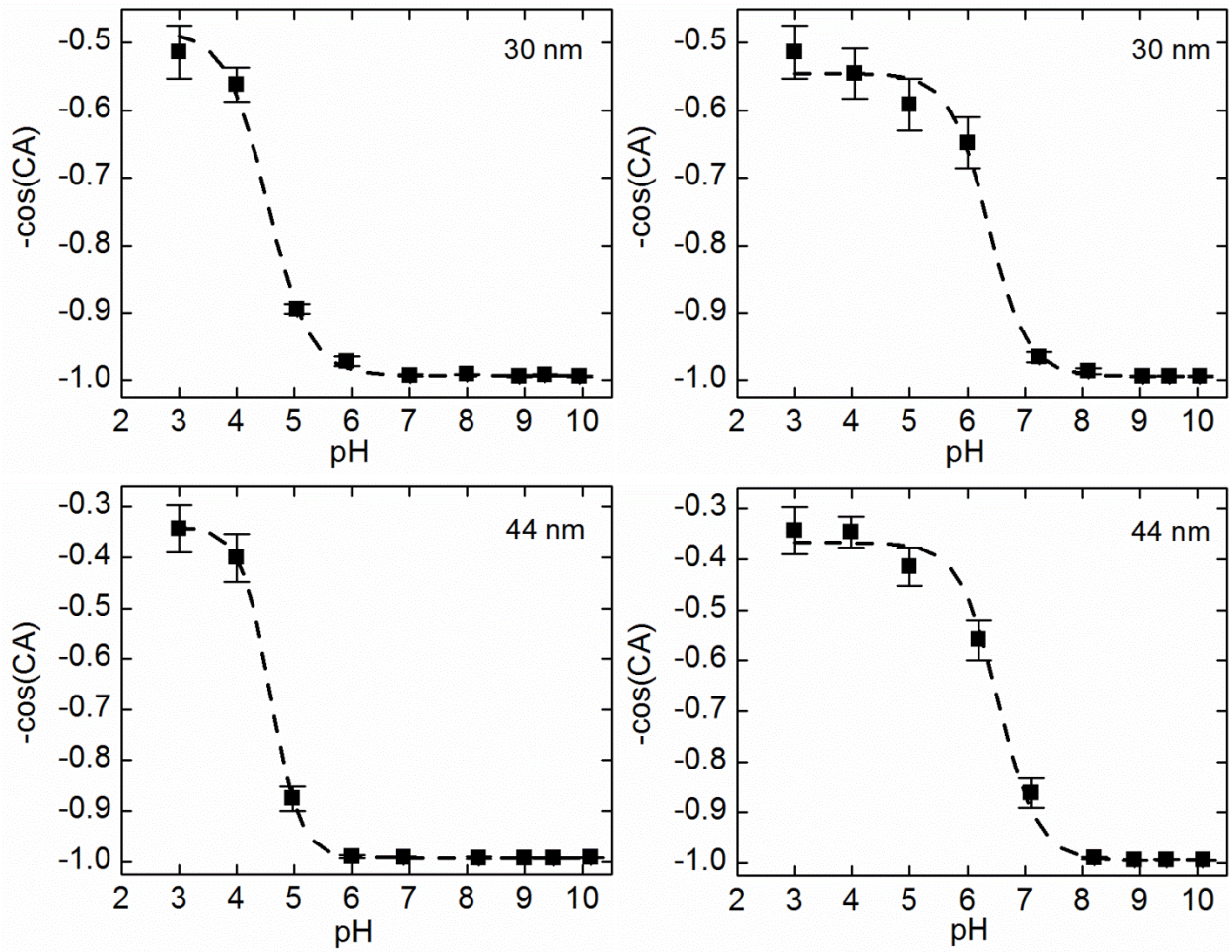

Figure S9. –cos(CA) as a function of pH for each brush thickness reported in Figure 2 (CA is the static water contact angle). Dry thickness (as-synthesized) is specified on each plot. In each pair of plots for a single thickness, the left graph corresponds to decreasing pH and the right graph corresponds to increasing pH. The dashed curves indicate sigmoidal fits to the data.

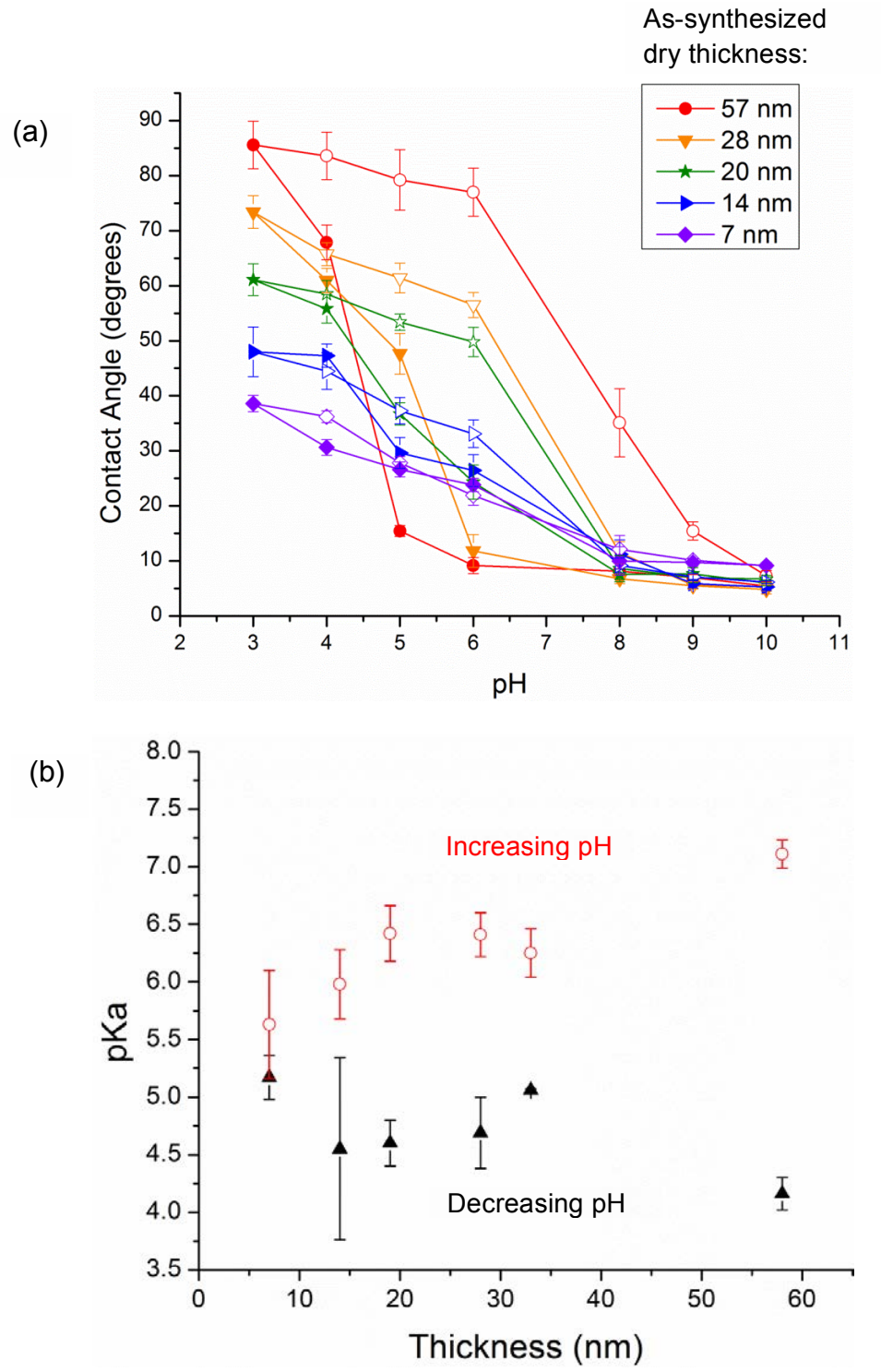

Figure S10. (a) Variation in water contact angle with pH measured for PAA brushes of varying thicknesses on glass substrates (grafting density = 0.32 chains/nm^2). (b) Variation in pK_a with as-synthesized dry brush thickness (○ increasing pH, ▲ decreasing pH). Data obtained for brushes grafted on glass surfaces exhibit a similar trend as that for brushes grafted on silicon wafers presented in the manuscript. Brushes were synthesized following procedures described in the main text, with the exception

that silicon substrates were replaced with glass coverslips. Brush parameters are shown in Table S3.

Table S3. Average as-synthesized dry thickness (with standard deviation) of each PtBA and PAA brush reported in Figure S10 (on glass substrates), corresponding molecular weight and dispersity of the PtBA that was polymerized in solution simultaneously during the PtBA brush synthesis, and reduction in brush thickness upon hydrolysis to PAA.

Average PtBA Brush Thickness (nm)	**M_n (kg/mol) of Solution PtBA (*Đ*)**	**Average PAA Brush Thickness (nm)**	**Reduction in PtBA Brush Thickness Upon Hydrolysis to PAA**
15.8 ± 0.2	28.9 (1.1)	7.3 ± 0.1	53.7 %
30.4 ± 0.3	57.9 (1.3)	14.3 ± 0.4	52.9 %
40.3 ± 0.2	82.2 (1.2)	19.5 ± 0.6	51.6 %
63.3 ± 0.5	117 (1.2)	27.8 ± 0.3	56.1 %
130.2 ± 0.4	248 (1.4)	56.7 ± 0.8	56.4 %

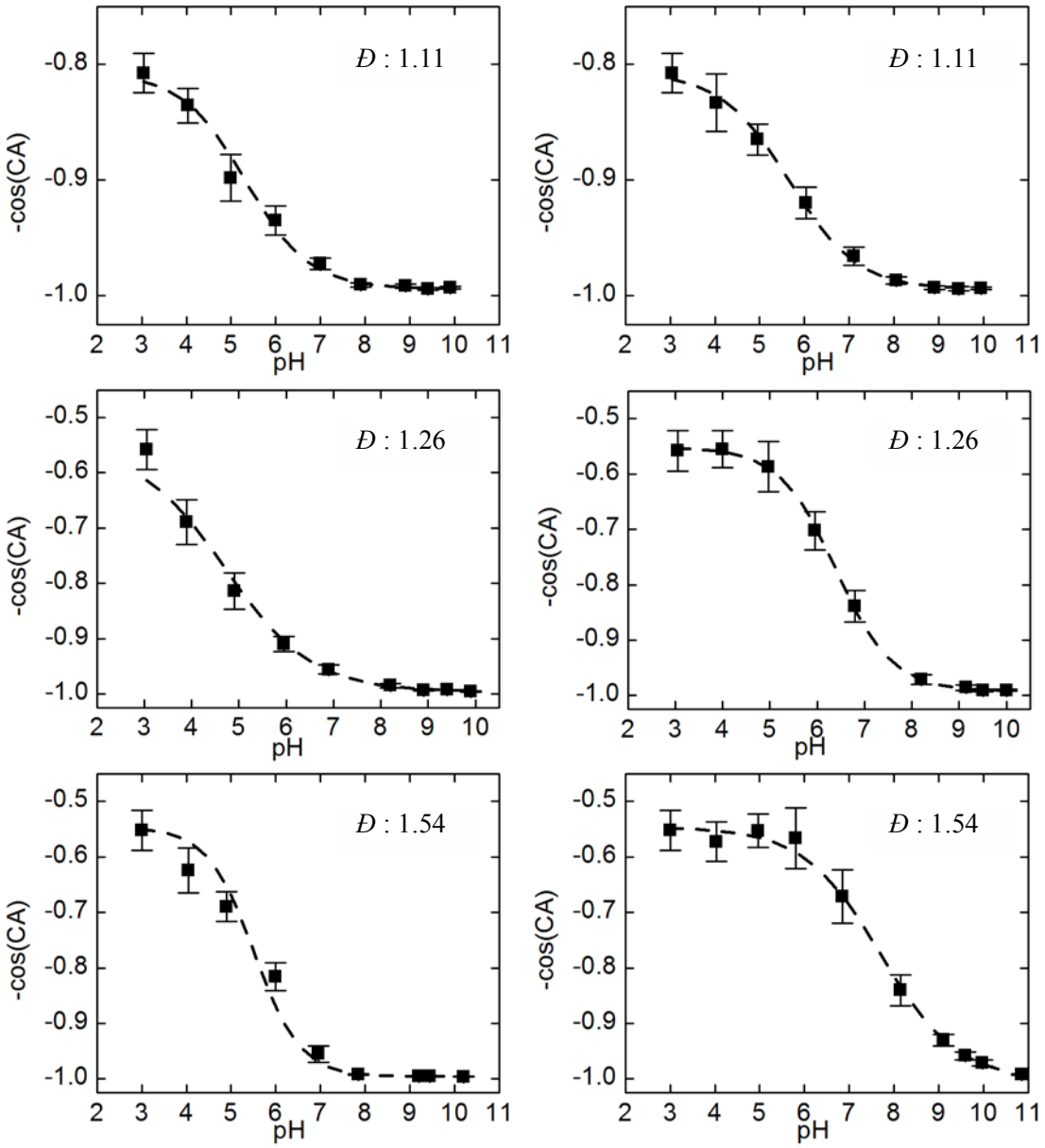

Figure S11. –cos(CA) as a function of pH for each brush reported in Figure 4(b) (CA is the static water contact angle). Solution PtBA dispersity is specified on each plot. In each pair of plots for a particular dispersity, the left graph corresponds to decreasing pH and the right graph corresponds to increasing pH. The dashed curves indicate sigmoidal fits to the data. In order to fit the data obtained upon decreasing pH, in which the low-pH contact angle plateau was not well-resolved, the low-pH contact angle value was fixed to that determined from the curve fit to the data obtained upon increasing pH. The error on the pK_a was taken to be the maximum value of standard error determined from the best fit curve (highest adjusted R^2 value).

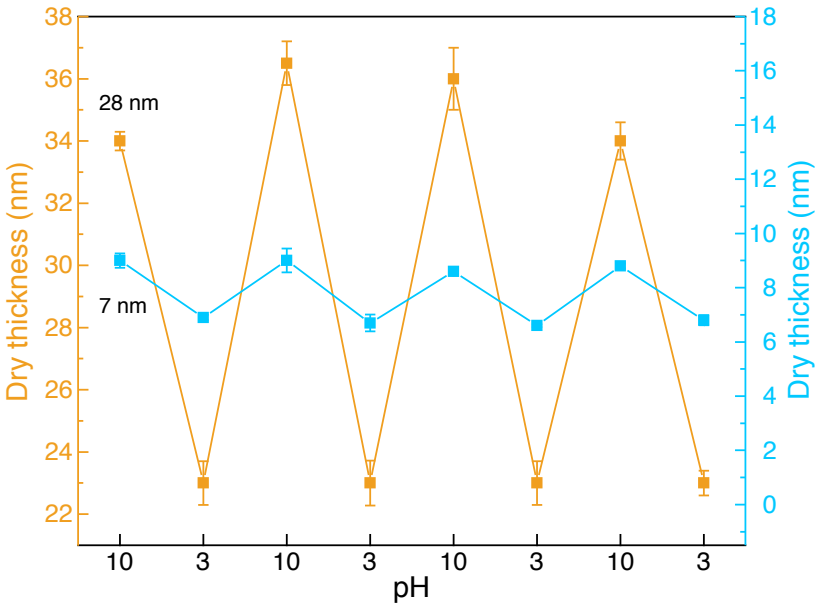

Figure S12. Reversible switching of PAA brushes with as-synthesized dry thickness of 28 nm (orange) and 7 nm (blue) (grafting density = 0.32 chains/nm^2). For each measurement, the brush was exposed to solution of the desired pH for 30 min. The error bars indicate the standard deviation across at least five measurements; the large variation in thickness (especially for the 28 nm brush) is attributed to the rapid switching between the two extreme pH values.

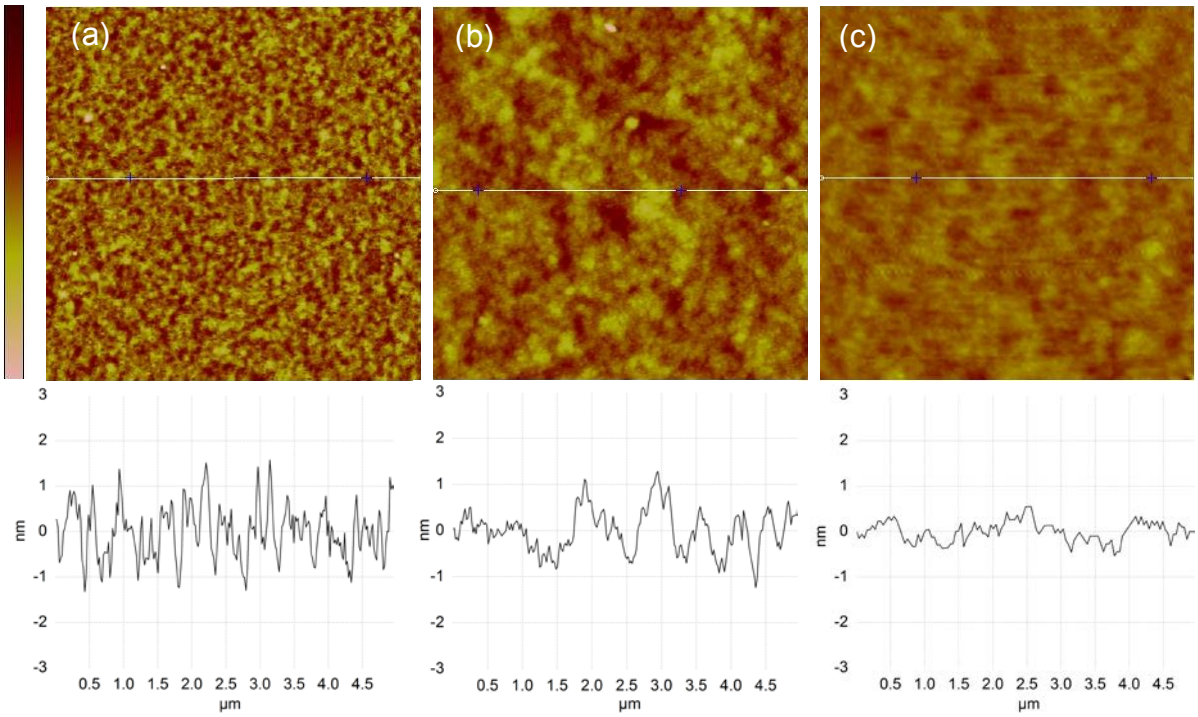

Figure S13. AFM images for (a) 27 nm PtBA brush on Si substrate, (b) 30 nm PAA brush on Si substrate, and (c) 12 nm PAA brush on Si substrate. The grafting density was 0.38 chains/ nm^2 for the 30 nm brush and was not measured for the other brushes. All images are 5 µm by 5 µm. The z-scale is 6 nm for all three images. The root-mean-square roughness is 0.29 nm, 0.48 nm, and 0.60 nm for the 12 nm, 30 nm, and 27 nm thick brushes, respectively. Typically, we find that the roughness decreases after hydrolysis of PtBA to PAA brush (as also observed by Lego *et al.*, Macromolecules, 2010, 43, 4384-4393).

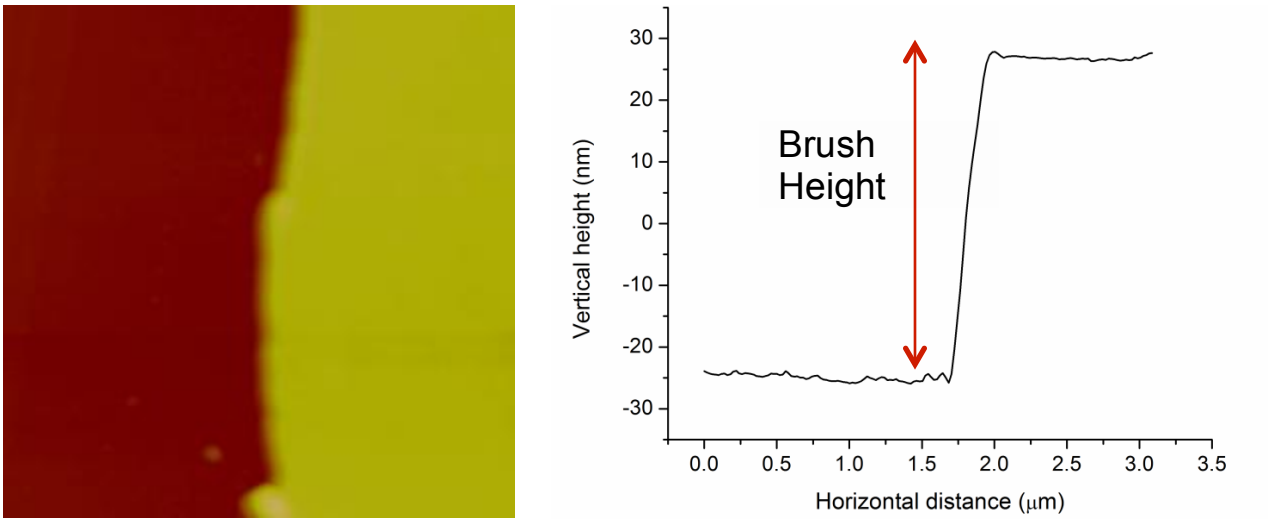

Figure S14. AFM image (5 μm × 5 μm) for 55nm PAA brush showing thickness measured after scratching the brush. Grafting density for PAA brush was 0.32 chains/nm^2.

Table S4. Static water contact angle as a function of soaking time for a PAA brush of as-synthesized dry thickness = 44 nm and grafting density = 0.47 chains/nm^2.

Soaking Time (min)	Contact Angle (degrees)	
	pH 3	pH 10
30	71.1 ± 0.8	8.3 ± 0.4
40	70.7 ± 0.6	9.0 ± 0.7
70	70.9 ± 1.1	7.9 ± 0.5

References

1. Balamurugan, S. S.; Subramanian, B.; Bolivar, J. G.; McCarley, R. L., Aqueous-Based Initiator Attachment and ATRP Grafting of Polymer Brushes from Poly(methyl methacrylate) Substrates. *Langmuir* **2012,** *28* (40), 14254-14260.
2. Lego, B. a.; Skene, W. G.; Giasson, S., Swelling Study of Responsive Polyelectrolyte Brushes Grafted from Mica Substrates: Effect of pH, Salt, and Grafting Density. *Macromolecules* **2010,** *43* (9), 4384-4393.
3. Wu, T.; Gong, P.; Szleifer, I.; Vlček, P.; Šubr, V.; Genzer, J., Behavior of Surface-Anchored Poly(acrylic acid) Brushes with Grafting Density Gradients on Solid Substrates: 1. Experiment. *Macromolecules* **2007,** *40* (24), 8756-8764.
4. Treat, N. D.; Ayres, N.; Boyes, S. G.; Brittain, W. J., A Facile Route to Poly(acrylic acid) Brushes Using Atom Transfer Radical Polymerization. *Macromolecules* **2006,** *39* (1), 26-29.
5. Kirwan, L. J.; Fawell, P. D.; van Bronswijk, W., In Situ FTIR-ATR Examination of Poly(acrylic acid) Adsorbed onto Hematite at Low pH. *Langmuir* **2003,** *19* (14), 5802-5807.
6. Dong, R.; Lindau, M.; Ober, C. K., Dissociation Behavior of Weak Polyelectrolyte Brushes on a Planar Surface. *Langmuir* **2009,** *25* (8), 4774-4779.
7. Sudre, G.; Hourdet, D.; Creton, C.; Cousin, F.; Tran, Y., pH-Responsive Swelling of Poly(acrylic acid) Brushes Synthesized by the Grafting Onto Route. *Macromolecular Chemistry and Physics* **2013,** *214* (24), 2882-2890.
8. Dai, J.; Bao, Z.; Sun, L.; Hong, S. U.; Baker, G. L.; Bruening, M. L., High-Capacity Binding of Proteins by Poly(Acrylic Acid) Brushes and Their Derivatives. *Langmuir* **2006,** *22* (9), 4274-4281.
9. Deng, S.; Ting, Y. P., Fungal Biomass with Grafted Poly(acrylic acid) for Enhancement of Cu(II) and Cd(II) Biosorption. *Langmuir* **2005,** *21* (13), 5940-5948.
10. Yu, H.-Y.; Xu, Z.-K.; Yang, Q.; Hu, M.-X.; Wang, S.-Y., Improvement of the antifouling characteristics for polypropylene microporous membranes by the sequential photoinduced graft polymerization of acrylic acid. *Journal of Membrane Science* **2006,** *281* (1–2), 658-665.
11. Suchoparek, M.; Spevacek, J., Characterization of the stereochemical structure of poly(tert-butyl acrylate) by one- and two-dimensional NMR spectroscopy. *Macromolecules* **1993,** *26* (1), 102-106.
12. Venkataraman, S.; Wooley, K. L., ATRP from an Amino Acid-Based Initiator: A Facile Approach for α-Functionalized Polymers. *Macromolecules* **2006,** *39* (26), 9661-9664.
13. Li, G.; Song, S.; Guo, L.; Ma, S., Self-assembly of thermo- and pH-responsive poly(acrylic acid)-b-poly(N-isopropylacrylamide) micelles for drug delivery. *Journal of Polymer Science Part A: Polymer Chemistry* **2008,** *46* (15), 5028-5035.
14. Liu, W.; Nakano, T.; Okamoto, Y., Stereochemistry of Acrylate Polymerization in Toluene Using n-BuLi. *Polym J* **1999,** *31* (5), 479-481.